RPE | Radiation Physics & Engineering
A Peer-Reviewed Journal
Published by K.N. Toosi University of Technology
http://rpe.kntu.ac.ir
Research Article

Radiation Physics and Engineering 2023; 4(3):29–41

Simulation of neutron and gamma shielding for an inertial electrostatic confinement fusion device

Hadi Zanganeh, Mahdi Nasri Nasrabadi*

Faculty of Physics, University of Isfahan, 81746-73441, Isfahan, Iran

HIGHLIGHTS

- Neutron and gamma shielding by layer method for IECF device.
- Calculation of necessary parameters and selection of suitable materials.
- Simulation of IECF device and its shield using MCNPX code.
- Dosimetry of different parts of the shield and the human environment.
- Dose Reduction of different parts to standard values and determining the optimal thickness for the shield.

ABSTRACT

In this work, neutron and gamma shielding were simulated using MCNPX code for an inertial electrostatic confinement Fusion (IECF) device. In this regard, various properties of shields were investigated. Portland reinforced concrete was considered as the first layer. In addition to being effective in reducing the dosage of fast neutrons, concrete layer was also considerably effective in reducing the dose of gamma rays. As for the second and third layers, we opted for paraffin and boric acid based. These layers were chosen based on parameters such as lethargy, macroscopic slowing down power (MSDP), etc. in order to reduce the speed of epithermal neutrons and then absorb the thermal neutrons, thus reducing the transmitted neutron dosage as much as possible. A layer lead was used after these three layers of shielding to attenuate the gamma ray reaching this layer. In this study, a fusion source based on D-T fuel with homogeneous and isotropic radiation of neutrons was used and then dosimetry was performed for different parts. Afterwards, the thickness of the shielding layers was optimized in such a way that the neutron and gamma doses were reduced according to the standards. We found that it is possible to achieve safe neutron and gamma fluxes and doses by applying about 5 layers of 50 cm thickness. We compared the results of our study with the those of another study done on shielding for the IECF device, which were in good agreement.

KEYWORDS

MCNPX code
IECF device
Neutron
Gamma
Dose
Flux
Shielding

HISTORY

Received: 14 February 2023
Revised: 12 April 2023
Accepted: 20 April 2023
Published: Summer 2023

1 Introduction

While the majority of research on fusion energy is focused on magnetic confinement, several alternative confinement methods have also been carried out, such as inertial electrostatic confinement Fusion (IECF) (Black et al., 2021). An IECF device is designed to perform nuclear fusion reactions together with other applications such as generating neutron, proton and X-ray (Chan and Herdrich, 2019; Farnsworth, 1966). However, this device cannot be used as a power device such as tokamaks (De Vries and Gribov, 2019; Spaeth et al., 2016). It has a relatively simple design and is also economical in terms of its usages and functions (Miley and Murali, 2014). These devices, like dense plasma focusing (DPF) equipment, are rich sources of high-energy electrons and ions, X-rays, and neutrons (Schmidt et al., 2014). Moreover, it has many applications in other fields such as medicine, industrial and research works. IECF device is a cylindrical device which is being developed as a tabletop neutron source (Syring and Herdrich, 2017). As a small neutron source, it can be used for neutron activation analysis, detection of landmines, neutron radiography, medical isotope production, plasma space propulsion and examining the properties of materials (Gueibe et al., 2022; Bhattacharjee et al., 2020; Damideh et al., 2012; Semsari et al., 2013).

*Corresponding author: mnnasrabadi@ast.ui.ac.ir

https://doi.org/10.22034/rpe.2023.384828.1116
https://dorl.net/dor/20.1001.1.26456397.2023.4.3.5.3

Among all mentioned applications, its applications as the source of neutron production are of crucial importance (Buzarbaruah et al., 2015, 2017, 2018). When neutrons are produced in the IECF as a result of nuclear fusion reactions such as D-T, as a consequence, neutron dose control is an essential matter for safety purposes. Therefore, in order to measure the rate of fast neutrons production by the IECF in a proper manner, it is necessary to explain the neutron transfer rate between an IECF and the radiation shield and the workplace where the neutron detector is located.

The Monte Carlo model is a suitable model to simulate particle collisions and calculate the energies left by them. One of the most important computational codes based on the Monte Carlo model is the MCNP code and one of the important codes for protecting neutron and gamma sources is the MCNPX code. To bring an example, the latter was used to build a shield for the Am-Be source (Nasrabadi and Baghban, 2013). Therefore, considering the hazards of radiations, we have designed suitable neutron and gamma shields in this study. We employed the MCNPX code to simulate neutron and gamma shields and performed dosimetry calculations. There are several studies that have used MCNP code to simulate neutron shields and so on (Werner et al., 2018; Werner, 2017; Pelowitz et al., 2013).

Concrete is one of the most well-known protective material. The composition of concrete has an important effect on its protective ability. The interaction between neutrons and the protective material depends on its energy and the density of the protective material. To improve the protective performance of concrete, an additional material can be mixed with it. The criteria for selecting the type of materials to increase the effectiveness of the interaction between neutrons and the material of shield must include some characteristics, namely high neutron scattering cross section as well as high density. Adding high density materials such as iron to concrete can improve its shield performance (Sariyer and Küçer, 2020; Bevelacqua and Mortazavi, 2020; Sariyer and Küçer, 2018). To improve the performance of neutron shields, a metal such as iron was added to the concrete layer of the shields, as confirmed by (DiJulio et al., 2016). Neutron has no electrical charge and its interaction with nuclei occurs via elastic and inelastic scattering, neutron capture, and nuclear fission and etc., while gammas interact mostly with orbital electrons and ionization of target atoms occurs due to the following interaction through photoelectric, Compton, and pair production phenomena. Consequently, the types of suitable materials for neutron shielding are quite different compared to those which are appropriate for gamma/X-rays shielding (Singh et al., 2015). Composites containing high atomic number materials such as Barium (Ba), Lead (Pb) and Bismuth (Bi) are utilized to absorb gammas or X-rays, while materials which contain low atomic number elements such as Hydrogen (H), Lithium (Li), Carbon (C), Boron (B), and Aluminum (Al) are preferred in absorbing neutron particles (Kaçal et al., 2019). Low atomic number elements with high scattering cross sections (the probability of neutron-target interaction) are found to be suitable for neutron attenuation and shielding (Okuno, 2005). Polyethylene and paraffin are often applied as basic materials for shielding small size sources, while for larger sources concretes and water are recommended as shielding materials (Zhang et al., 2017). High-density concretes containing both high atomic number materials and boron-enriched materials have been recommended for shielding both gamma-rays and neutrons (Mesbahi and Ghiasi, 2018; Naseri and Mesbahi, 2010).

Our goals in this research are firstly to find suitable materials for neutron and gamma shielding for IECF device of University of Isfahan (Salehizadeh and Nasrabadi, 2021), and secondly to simulate the best geometry for shielding and doing dosimetry calculations to guarantee the safety of different users' workplace with MCNPX code, and finally to prepare the conditions for setting up and using this device. For an exact shielding, it should obtain a realistic picture of geometry, location of detectors and other involving parameters. It is necessary to calculate the dose and flux of neutrons and gammas in all cells. Therefore, the MCNPX code was used in order to calculate these parameters. In this study, we tried to find some approaches to improve the shielding and all parameters, which can be obtained from experimental values and the other methods. Most of the published articles about shielding the IECF devices are for D-D fuel, where the energy of neutrons produced by this reaction is 2.45 MeV, but in this study, we have simulated shielding for a D-T fuel, where the energy of neutrons produced by this reaction is 14.1 MeV and despite this difference in neutron energy in this reaction, the thickness we obtained in the shielding simulation is in agreement with and close to the results of the reference paper.

2 Material and Methods

In shield structure, we have a combination of neutron and gamma fields. Each of these has its own interactions. So we have to consider specific geometric arrangements for each of them. There are several ways to design shields, including neutron and gamma layer shields (Sazali et al., 2019). In the second method, after selecting different suitable materials for neutron and gamma shielding, we combine them to create a unit shield that is called a homogeneous shield (Pomaro et al., 2019). In shield construction, we can have a combination of methods 1 and 2 at the same time (both a homogeneous shield and a layered shield). Here, we chose the layered shielding method. The steps of constructing the shield in this method were as follows: 1) Since the neutrons of the IEC device are fast neutrons, we chose the first layer of protection from a material that reduces the population of fast neutrons (Hu et al., 2020) as much as possible. 2) For the second layer of protection, we chose a material that slows down the neutrons (Santosa and Anggraini, 2018). 3) For the third layer of the shield, we chose a material that absorbs neutrons that were slowed down and became thermal in the previous layers (Zan et al., 2020). 4) In this step we chose a material to absorb the gammas that reach this layer. 5) In this step we chose a material that reflects the

thermal neutrons which reach this distance (Stone et al., 2019). There are three important parameters in choosing the first material of the shield: 1) Determining the threshold energy of the inelastic scattering of that material. 2) Determining the cross sections of the inelastic scattering of neutrons with that material. 3) Reviewing the manufactured by-products. According to Table 1, we compared the inelastic scattering threshold energy of different materials.

According to Table 1, iron has one of the lowest inelastic scattering threshold energies, so it is more useful in controlling high-energy neutrons. As mentioned earlier, the presence of metal in the shield layers helps control high-energy neutrons. For the first layer of the shield, we chose Portland reinforced concrete. In the next step, the cross section of the inelastic scattering of neutrons with materials, for instance for Fe, was obtained (Fig. 1).

To select the material of the moderator layer, we also considered some important properties, including: 1) the appropriate elastic scattering cross section, 2) lethargy, 3) MSDP, and 4) Thermalize Factor (TF). Lethargy is the mean decrement of the logarithm of the energy of a neutron passing through the matter in the slowing down process and is given by Eq. (1). A good moderator should possess a high average energy reduction for neutrons (Zakalek et al., 2021). Table 2 lists the lethargy values for some materials in case for comparison. For calculating the lethargy of elements, we use Eq. (1), in which A is the mass number of the desired nucleus. If the slowing-down medium contains n kinds of nuclides, each of the microscopic scattering cross section σ_s and average logarithmic energy decrement ς, the mean value of ς for the n species is given by of Eq. (2).

$$\varsigma = 1 + \frac{(A-1)^2}{2A}\ln(\frac{A-1}{A+1}) \quad (1)$$

$$\varsigma = \frac{\sum_{i=1}^{n}\sigma_{si}N_i\varsigma_i}{\sum_{i=1}^{n}\sigma_{si}N_i} \quad (2)$$

As can be seen in the Table 2, water, boron and paraffin with high lethargy were chosen. Another parameter to study the moderator material is MSDP which is given as below (Lamarsh, 1966):

$$\text{MSDP} = \varsigma\Sigma_s \quad (3)$$

where Σ_s is the elastic scattering cross section. High MSDP is another property of a good moderator, whose value for some materials is given in Table 3.

According to Table 3, paraffin has the highest amount of MSDP, which shows that it is a suitable material for the second layer. In Table 4, the lethargy and MSDP parameters were compared and the best materials for the second layer of shields were selected.

Based upon Table 4, paraffin and light water have the best values of these two parameters in order to be used in the moderator layer. Another indicator of the choice of moderator material is TF, which its value for different materials is given by the following equation:

$$TF = \frac{\text{Fast neutron yield } (\text{s}^{-1})}{\text{Thermal neutron flux } (\text{cm}^{-2}.\text{s}^{-1})} \quad (4)$$

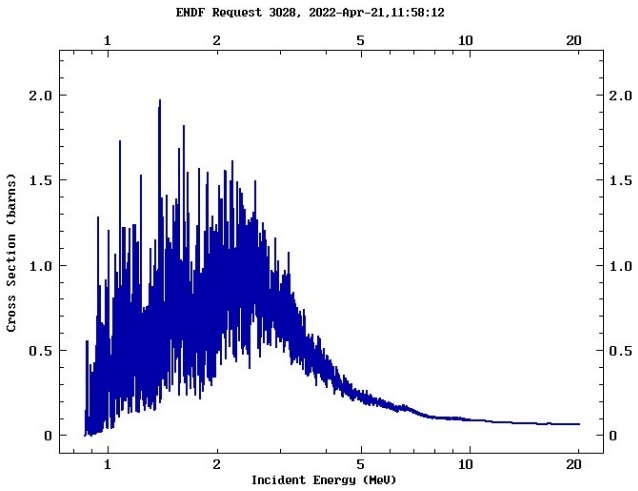

Figure 1: Inelastic cross section of Fe-56 (ENDF, 2022).

Table 1: Inelastic scattering threshold energy (ENDF, 2022).

Material	Inelastic scattering threshold energy (MeV)
Fe	$E_b \leq 2.10$
Al	$E_b \approx 2.25$
Pb	$E_b = 3.20$
C	$E_b = 4.80$
O	$E_b = 6.60$

Table 2: Calculated lethargy of materials.

Material	Lethargy
H_2O	0.927
D_2O	0.510
Be	0.207
$C_{25}H_{52}$	0.910
BeO	0.180
He	0.427
B	0.171
C	0.158

Table 3: Macroscopic Slowing Down Power.

Material	MSDP
H_2O	1.425
D_2O	0.176
Be	0.158
$C_{25}H_{52}$	1.690
BeO	0.130
He	1.6×10^{-5}
B	0.092
C	0.060

Table 4: The Lethargy MSDP Comparison (Bell and Glasstone, 1970).

Material	Lethargy	MSDP
H_2O	0.927	1.425
D_2O	0.510	0.176
Be	0.207	0.158
$C_{25}H_{52}$	0.910	1.690
BeO	0.180	0.130
He	0.427	1.6×10^{-5}
B	0.171	0.092
C	0.158	0.060

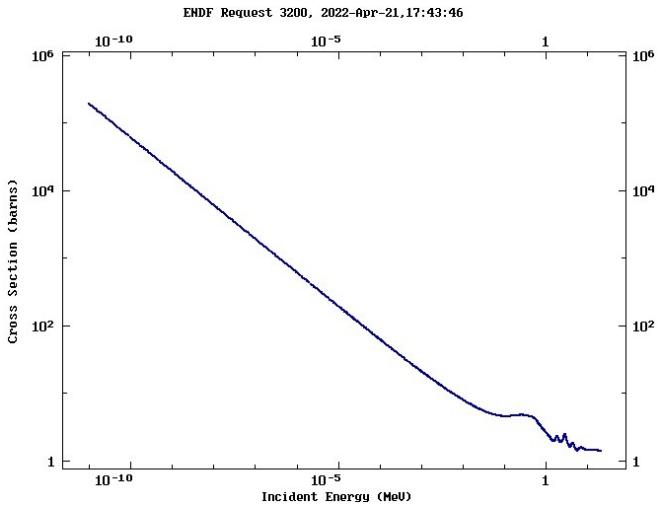

Figure 2: Thermal absorption cross section of B-10 (ENDF, 2022).

The materials selected for shielding should have small values of the Thermalize Factor (TF) parameter. In the third step, in order to choose the absorbers of thermal neutrons which must have the maximum amount of neutron absorption cross section, materials such as B-10, Li-6, Li-7, Gd-152, Xe-135, Cd-113 are selected as the best materials. In the next step, we should add a gamma attenuating layer for shielding. Figure 2 shows the cross-sectional area of thermal absorption for B-10 (Lamarsh, 1966).

According to Fig. 2, due to the cross-sectional area of the thermal adsorption of B-10, we found it suitable for the third layer of the shield. Boron is also used in nuclear reactors to absorb thermal neutrons to reduce reactors power. To select the fourth layer of the shield, we should have a gamma attenuating layer for shielding. In the next step, in order to design the shielding, we also needed to control the gamma dose rate. In this regard, we considered features such as the half-value layer (HVL) for the shield. This parameter is obtained from the following equation (Stults and Karpius, 2021; El-Toony et al., 2020; Asadi and Hosseini, 2021).

$$I = I_0 \mathrm{e}^{-\mu x} \tag{5}$$

where $x_{HVL} = \ln 2/\mu$, x is the thickness of the shield desired, i_0 is the initial intensity of the radiation beam and μ is the linear attenuation coefficient. Table 5 shows the linear attenuation coefficient for several materials.

According to Table 5, for several elements, the linear attenuation coefficient (μ) is different and by an increase in the energy of beam, μ decreases. Pb and Concrete have the maximum value of μ and can be a good choice to decrease the energy of gamma beam. Table 6 shows the HVL values for three different gamma energies and different materials according to which we selected the fourth layer material.

According to Table 6, based on this factor, lead is the suitable choice for the shield layer that should be used to attenuate photons. According to Table 6, the materials described above for the different layers of shield were selected and used in different thicknesses in our simulations. Some of these materials had dual or multiple uses for us, such as reinforced concrete, which reduced both the neutron and the gamma doses. Based on above parameters we selected the first layer of shield Portland reinforced concrete to create large dispersions for the fast neutrons produced. This layer, in addition to being able to reduce the neutron dose well, has also had a great effect in reducing the gamma dose, which is another advantage of using this type of concrete. We chose the second layer to slow down the neutrons to absorb in the next layer. In the third layer, paraffin was able to reduce the neutron dose to an appropriate amount to be absorbed by reducing the energy of neutrons and convert them into thermal neutrons. We selected the third layer of boric acid to absorb the thermal neutrons that reached this thickness to the maximum because boron has a high cross-sectional area of thermal neutrons, which was reduced by measuring the neutron dose. We chose lead for the fourth layer to control the gamma dose, which by measuring the gamma dose, this layer was able to reduce the gamma dose well. We also reached the last layer to reflect the thermal neutrons so that we chose this thickness to act as a reflector of these neutrons inside the shields. However, it is possible to choose other materials and the number of these choices can be very large. The list of materials used in our simulations is given in Table 7.

3 Simulation

After studying the physics of the problem and selecting the appropriate materials, we proceeded to the simulation of different shield layers for the IECF device using the MCNPX code. MCNPX is a powerful code to simulate shielding for various neutrons, gamma and other sources. First we designed the geometry of the shield. Then we studied and simulated a neutron source that is compatible with the IECF device of the University of Isfahan. Then we performed dosimetry calculations to measure the stopping power of the simulated shields.

3.1 Geometry design

In this step of simulation, we first simulated the geometry of the shields. Due to the fact that the anode geometry of the IECF device is cylindrical, we thought it would be better to design the different layers of protection geometrically cylindrical, because they will have perfect symmetry with the source chamber, which is the best case. Figure 3 is the two-dimensional (2D) images of the simulated geometry.

Figure 3 shows the order of the different layers of the simulated shield and the different dimensions of the shield in two dimensions. Figure 4 shows the names of the materials used and the sizes and thicknesses used in the simulation of the IECF device. We designed the geometry dimensions so precisely that from the point of view of all the plates, the distances of the shields correspond exactly to the thickness of the different layers of shields, both around the cylinders and at the top and bottom of the cylinders.

Table 5: Linear attenuation coefficient (μ) per cm^{-1} (Hubbell and Seltzer, 1995).

Material	ρ ($g.cm^{-3}$)	Energy (MeV)										
		0.1	0.2	0.3	0.5	0.8	1	2	3	5	8	10
C	2.25	0.335	0.274	0.238	0.196	0.159	0.143	0.100	0.080	0.061	0.048	0.044
Al	2.70	0.435	0.324	0.278	0.227	0.185	0.166	0.117	0.096	0.076	0.065	0.062
Fe	7.90	2.720	1.090	0.838	0.655	0.525	0.470	0.335	0.285	0.247	0.233	0.232
Cu	8.90	3.800	1.309	0.960	0.730	0.581	0.520	0.372	0.318	0.281	0.270	0.271
Pb	11.35	59.700	10.150	4.020	1.640	0.945	0.771	0.516	0.476	0.482	0.518	0.522
Air	1.21×10^{-3}	1.95×10^{-4}	1.59×10^{-4}	1.37×10^{-4}	1.12×10^{-4}	9.12×10^{-5}	8.45×10^{-5}	5.75×10^{-5}	4.60×10^{-5}	3.54×10^{-5}	2.84×10^{-5}	2.61×10^{-5}
H_2O	1	0.167	0.136	0.118	0.097	0.079	0.071	0.049	0.040	0.030	0.024	0.022
Concrete	2.35	0.397	0.291	0.251	0.204	0.166	0.149	0.105	0.085	0.067	0.057	0.054

Table 6: HVL for several beam energy (E_b) of gamma rays.

Material	HVL For 100 keV (cm)	HVL For 200 keV (cm)	HVL For 500 keV (cm)
Air	3555	4359	6189
H_2O	4.15	5.1	7.15
C	2.07	2.53	3.54
Al	1.59	2.14	3.05
Fe	0.26	0.64	1.06
Cu	0.18	0.53	0.95
Pb	0.012	0.068	0.42

Table 7: List of materials used in our simulations.

Material	Composition	Atom Fraction	Density ($g.cm^{-3}$)	Chemical Formula
Air	C	0.000150	0.001205	-
	N	0.784431		
	O	0.210748		
	Ar	0.004671		
Stainless Steel	C	0.003405	7.860000	-
	N	0.004866		
	Si	0.009708		
	P	0.000528		
	S	0.000255		
	Cr	0.188773		
	Mn	0.086851		
	Fe	0.065916		
	Ni	0.046454		
Reinforced concrete (iron-Portland concrete)	H	0.135585	5.900000	-
	O	0.150644		
	Mg	0.002215		
	Al	0.005065		
	Si	0.013418		
	S	0.000646		
	Ca	0.040919		
	Mn	0.002638		
	Fe	0.648869		
Paraffin	H	0.675311	0.930000	$C_{25}H_{52}$
	C	0.324689		
Boric Acid	H	0.428571	1.500000	H_3BO_3
	B	0.142857		
	O	0.428571		
Lead	Pb	1.000000	11.350000	Pb
Cadmium	Cd	1.000000	8.650000	Cd

3.2 Source design

After designing the geometry, we designed the neutron source in accordance with the IECF device. In the IECF device inside the anode, there is a cathode. The shape of the cathode is a spherical grid. As shown in Fig. 5, positive and negative voltages are applied to the anode and the cathode respectively.

After applying the voltage to the anode and cathode, a potential well is created inside the device according to Fig. 6, the center of the potential well is spherical grid, and fuel injection and ionization cause the ionized fuel

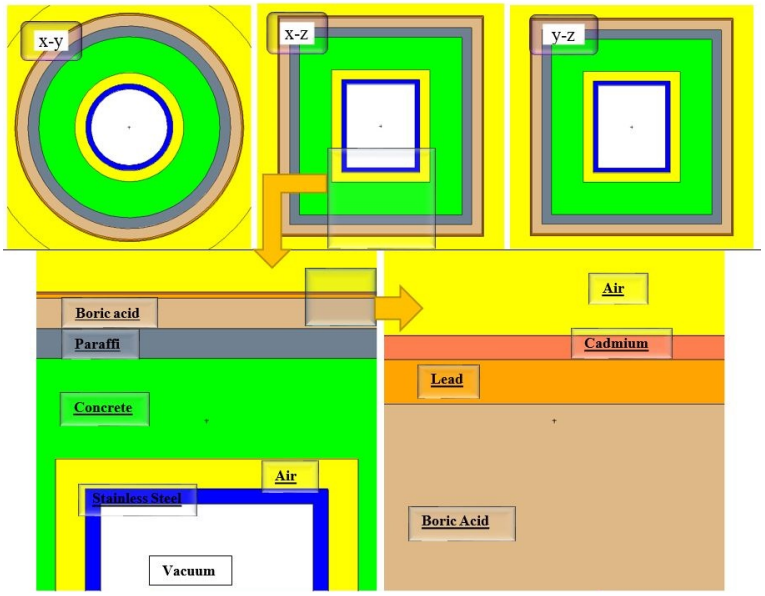

Figure 3: 2D simulated geometry ($x-y$ plane), ($x-z$ and $y-z$ plane).

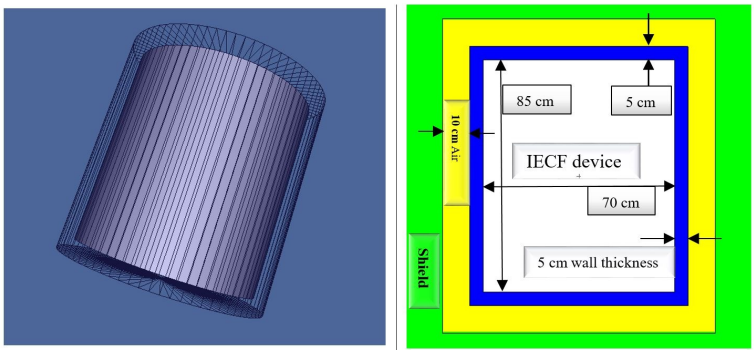

Figure 4: Dimensions and geometry size of the IECF device.

particles to fall into the potential well. In fact, most of the fuel particles go into the spherical grid.

After a short time, in the ion-neutral collisions, in the center of the device IECF, electrons separate from neutral particles and create a virtual anode with all the ions in the center of spherical grid shown in Fig. 7. Then, because of the released electrons, we will also have virtual cathodes at the same time with virtual anodes in the center of the well.

Therefore, according to the Fig. 7, trapping the fuel particles occur between these virtual anodes and cathodes, and the collision between these particles, which leads to fusion and production of neutrons, takes place in the center of the device and in a spherical grid, and their state becomes spherical due to the virtual anodes and cathodes. Therefore, the source was simulated as a spherical volumetric source. For source energy, we used the fusion function (Gaussian function) defined for the fusion source in the MCNPX code. The energy spectrum of all neutrons produced from this source is 14.1 MeV. We considered the angular distribution of the neutron radiation from the source to be isotropic in all directions based on reality and the intensity of the source (10^9 s^{-1}).

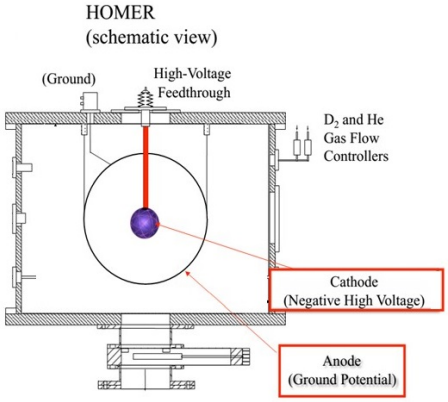

Figure 5: Anode and cathode voltages of IECF device.

3.3 Dosimetry calculations

In dosimetry calculations, we used different tallies of MCNPX code. Tally F4 or F5 was examples of tallies used to calculate neutron and gamma doses in different layers of shields. We used point and ring detectors in different layers and around the device to measure neutron and photon fluxes for dosimetry calculations.

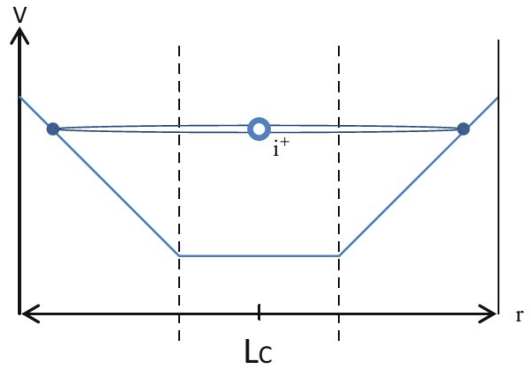

Figure 6: Potential well created after voltage is applied.

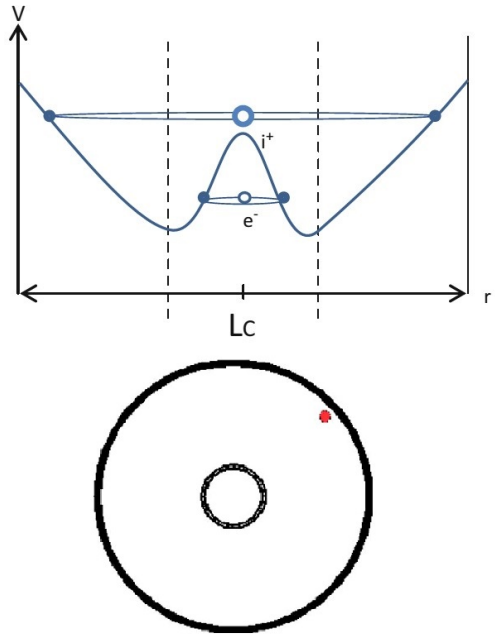

Figure 7: Virtual spherical cathodes and anodes shells.

4 Results and discussion

Neutron protection is based on the slowing down of fast neutrons and then their absorption. Here, we investigated suitable materials to slow down and then absorb neutrons, in addition to absorbing gamma. After achieving the best combination of materials described in the previous sections, based on their effective thicknesses, we measured the values of flux and neutron and photon doses after passing through these shield layers, and measured and reduced them to safe and standard values as defined in ICRP60. In the table below, we have listed different thicknesses of selected materials. In Table 8, we showed the different thicknesses we used to simulate the shield. We added the thicknesses in order of 2 cm and performed the calculations.

As can be seen in Table 8, the most changes have been made to reinforced concrete, which is the first layer of the shield, and then the other two materials have changes in thickness. Based on Table 8, Fig. 8 shows neutron dose for different thicknesses of the layers that is calculated by DF4. It has been done on cells number 4 to 8. The percentage error of the simulation calculations with the MCNPX code, which is shown in Figs. 8 to 14, was always less than 5%.

According to Fig. 8, the maximum neutron dose reduction occurs by increasing the concrete thickness, i.e. Portland reinforced concrete has the most neutron dose reduction, and then the second and third 10 cm, i.e. paraffin and boric acid, reduce the neutron dose to our expected level. In Fig. 9, we also calculated the neutron surface dose rate values for different thicknesses with F2 tally that modified by DF2.

As can be seen in Fig. 9, the largest decrease in neutron dose rate occurred during the increase in the thickness of Portland reinforced concrete, and this calculation of surface neutron dose rate also confirms the results of volumetric neutron dose rate calculations calculated with F4 tally in the previous figure. Figure 10 shows the amount of photon dose reduction at different thicknesses.

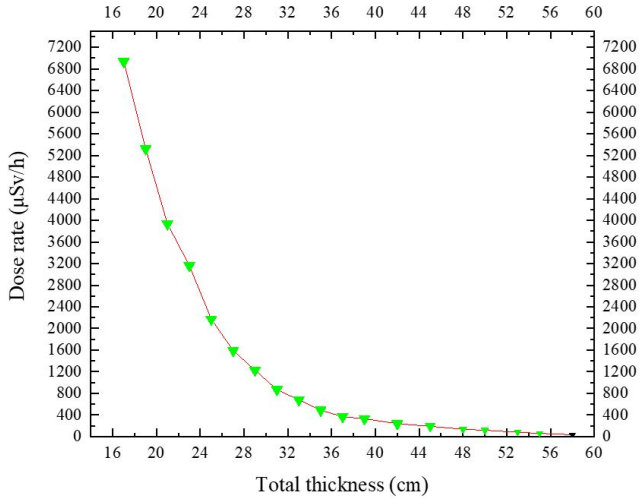

Figure 8: Neutron dose rate in the shield by F4 Tally.

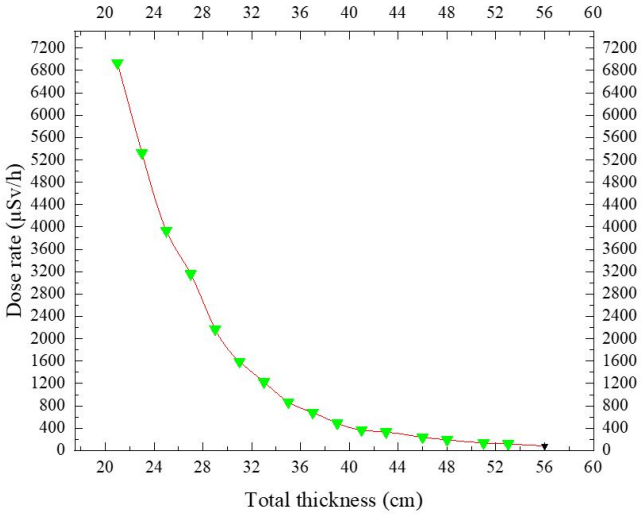

Figure 9: Neutron surface dose calculation in the shield by F2 Tally.

Table 8: List of materials used in the simulations.

Total thickness (cm)	Iron-Portland Concrete (cm)	Paraffin (cm)	Boric Acid (cm)	Lead (cm)	Cadmium (mm)
17	5	5	5	1.3	7
19	7	5	5	-	-
21	9	5	5	-	-
23	11	5	5	-	-
25	13	5	5	-	-
27	15	5	5	-	-
29	17	5	5	-	-
31	19	5	5	-	-
33	21	5	5	-	-
35	23	5	5	-	-
37	25	5	5	-	-
39	27	5	5	-	-
42	30	5	5	-	-
45	33	5	5	-	-
48	36	5	5	-	-
50	36	7	5	-	-
53	36	10	5	-	-
55	36	10	7	-	-
58	36	10	10	-	-

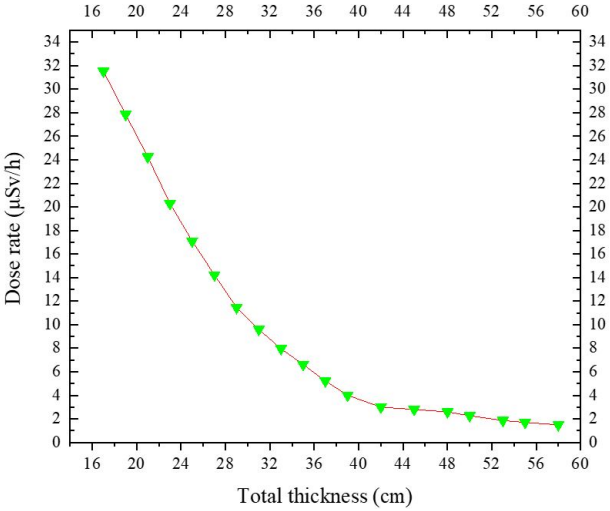

Figure 10: Gamma dose rate in the shield by F4 Tally.

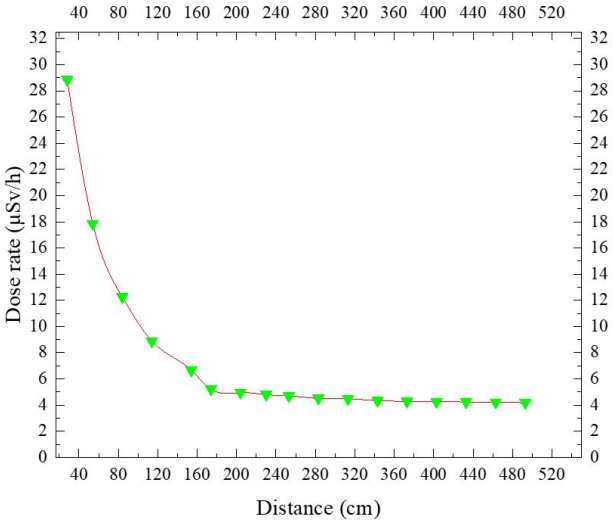

Figure 11: Neutron dose rate calculation at room by F4 Tally.

The maximum gamma dose was inhibited by using 3 cm of lead but despite the constant thickness of the lead, it can be seen that the gamma dose also is decreased with the thickness increase of the Portland iron concrete. The presence of iron in concrete is one of the main reasons for this sharp drop, which has largely controlled high-energy neutrons. As the thickness of the concrete stabilizes and the thickness of the paraffin and boric acid increases, the gamma dose remains almost constant. This means that the concrete has a positive effect on reducing the gamma dose. Finally, the photon dose is reduced below its standard value. All these simulations enable us to operate IECF device with safety. For this purpose, the neutron and gamma dose and the total dose must reach the permitted level specified in ICRP60 in the workplace where the device is located. In Fig. 11, after finishing the shield layers, we measured the neutron and then the gamma dose values by the appropriate tallies, inside the workplace where users have to work with the device.

According to Fig. 11, in the first 40 cm and close to the device, the neutron dose is about 30 μSv.h^{-1}, which decreases with increasing user distance from the device, so that at a distance of 40 to 160 cm (for a height of 400 cm), this dose decreases to about 17 to 5 μSv.h^{-1}. From a distance of 160 cm to about 280 cm from the device and beyond, the neutron dose drops to about 4 μSv.h^{-1}. In Fig. 12, the neutron dose rate in the workplace was obtained based on Tally F2, which is modified by DF2 to give the surface neutron dose rate.

To calculate F2 tally in the workplace where the device is located and the user is present, we considered surfaces at distances of 20 to 30 cm and obtained the surface neutron dose by F2 tally. The calculated error for this tally for different surface distances was in the range of 1 to 6%. The importance of calculating the neutron dose rate in the workplace where the user is present, made us obtain the neutron dose values, which is the most effective dose, from

two methods (F2 and F4 tallies) and to compare them with each other in order to make our simulation more accurate. Figure 13 also shows the amount of gamma dose at different distances from the device inside the room.

The amount of gamma dose is much less than the neutron dose and this dose is completely safe for different distances from the device. In Fig. 14, we have calculated the total dose, including neutron and gamma doses for different distances in the room.

As can be seen in Fig. 14, the gamma dose has less effect on the total dose and the main dose is related to the neutron. Figure 15 shows the decrease in the flux of fast, epithermal and thermal neutrons while passing through different layers of shield thickness.

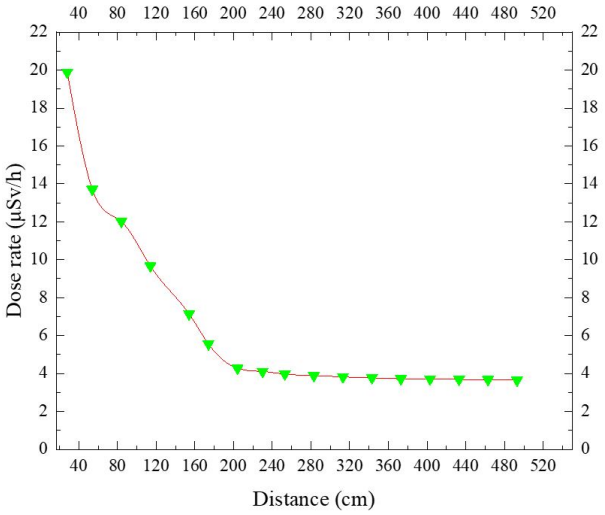

Figure 12: Neutron dose rate calculation at room by F2 tally.

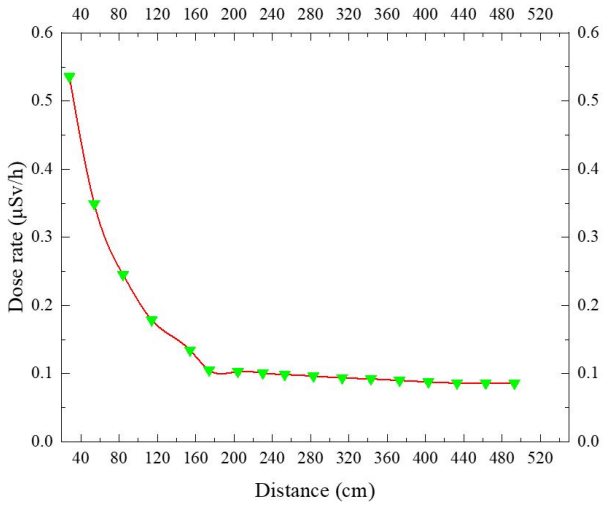

Figure 13: Gamma dose rate calculation at room by F4 tally.

In Figure 15, at the beginning of the first layer, which is made of concrete, at a thickness of 10 cm, the flux of fast neutrons shows a large decrease, while the flux of epithermal and thermal neutrons increases from the thickness 10 to 16 cm. At thicknesses of about 14 and 16 cm, respectively, the flux of epithermal and thermal neutrons starts to decrease. According to Fig. 15, the thickness of the first layer has been able to reduce the flux of fast neutrons, and finally, all three ranges of neutron flux are well close to zero. In Table 9, we calculated the total neutron dose rate outside the shield layers for all different shield thicknesses inside the workplace where the IECF device is located. We have calculated these neutron dose rates based on the distance that the user may have from the device.

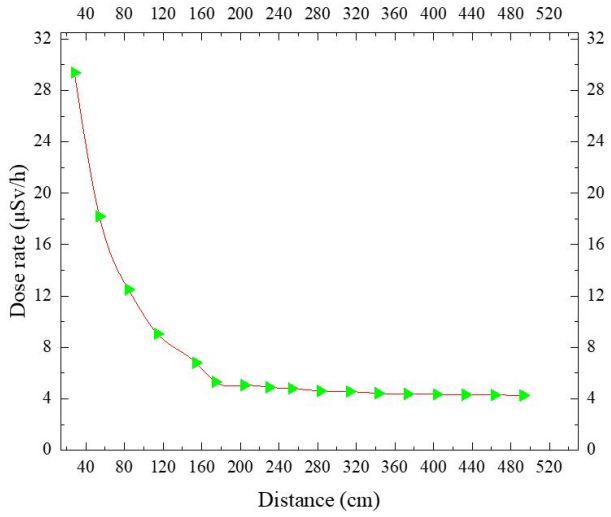

Figure 14: Total dose rate calculation at room by F4 tally.

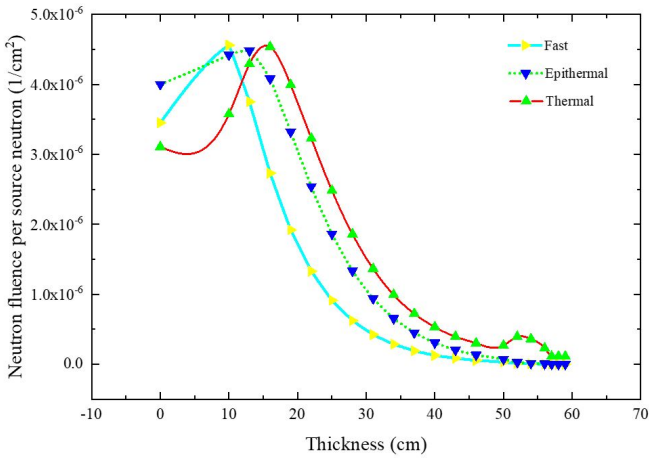

Figure 15: Fluence of neutrons by passing through different layers of the shield by F4 tally.

As can be seen in Table 9, by increasing all the thicknesses of the shields, the neutron dose rate for all distances between the user and the device, the neutron dose rate has reduced. But for each thickness of the shields, at some distances the neutron dose rate is safe, and at some distances close to the device is dangerous according to ICRP60 standards for long working hours. For the thicknesses of about 46 to 48 cm and more, the neutron dose rate is suitable for long working hours with the device at different distances. The best obtained thickness of the different layers of the shield in this simulation is 56 cm which is the safest neutron dose rate for long working hours. This issue is also

Table 9: Calculated total dose rate ($mSv.h^{-1}$) of neutron in all thicknesses.

Thickness (cm)	Distance (cm)							Error (%)
	33	63	89	119	149	179	305	
21	2.67	1.38	8.89	6.23	4.52	3.43	2.69	0.76
23	2.12	1.09	7.02	4.91	3.56	2.70	2.12	0.80
25	1.64	8.66	5.55	3.89	2.81	2.13	1.67	0.95
27	1.28	6.84	4.37	3.06	2.21	1.67	1.31	1.01
29	9.89	5.41	3.45	2.41	1.74	1.32	1.03	1.14
31	7.65	4.28	2.72	1.90	1.37	1.04	8.16	1.28
33	5.90	3.38	2.14	1.49	1.08	8.16	6.40	1.45
35	4.62	2.69	1.70	1.18	8.52	6.45	5.06	1.64
37	3.56	2.11	1.34	9.31	6.70	5.06	3.96	1.82
39	2.72	1.65	1.04	7.28	5.25	3.95	3.09	2.09
41	2.10	1.30	8.18	5.70	4.12	3.09	2.42	2.32
43	1.62	1.02	6.42	4.46	3.22	2.42	1.89	2.62
46	1.10	7.12	4.44	3.09	2.20	1.66	1.29	3.09
48	8.71	5.74	3.56	2.47	1.77	1.33	1.03	3.47
51	6.48	4.43	2.75	1.92	1.37	1.04	8.11	3.96
53	5.31	3.72	2.30	1.60	1.13	8.56	6.67	4.28
56	2.83	1.75	1.20	8.67	6.52	5.09	4.59	4.86

Table 10: Calculated the total dose rate ($mSv.h^{-1}$) of gamma in all thicknesses.

Thickness (cm)	Distance (cm)							Error (%)
	33	63	89	119	149	179	305	
21	1.01×10^{-2}	5.42×10^{-3}	3.53×10^{-3}	2.50×10^{-3}	1.83×10^{-3}	1.39×10^{-3}	1.09×10^{-3}	1.43
23	9.28×10^{-3}	5.01×10^{-3}	3.25×10^{-3}	2.30×10^{-3}	1.68×10^{-3}	1.28×10^{-3}	1.00×10^{-3}	1.54
25	8.57×10^{-3}	4.73×10^{-3}	3.08×10^{-3}	2.17×10^{-3}	1.59×10^{-3}	1.22×10^{-3}	9.51×10^{-4}	1.62
27	7.44×10^{-3}	4.19×10^{-3}	2.72×10^{-3}	1.92×10^{-3}	1.39×10^{-3}	1.06×10^{-3}	8.36×10^{-4}	1.82
29	6.45×10^{-3}	3.69×10^{-3}	2.40×10^{-3}	1.68×10^{-3}	1.22×10^{-3}	9.37×10^{-4}	7.32×10^{-4}	2.22
31	5.55×10^{-3}	3.25×10^{-3}	2.11×10^{-3}	1.48×10^{-3}	1.07×10^{-3}	8.26×10^{-4}	6.43×10^{-4}	2.55
33	4.55×10^{-3}	2.72×10^{-3}	1.76×10^{-3}	1.23×10^{-3}	8.91×10^{-4}	6.77×10^{-4}	5.36×10^{-4}	2.87
35	3.97×10^{-3}	2.42×10^{-3}	1.56×10^{-3}	1.10×10^{-3}	7.93×10^{-4}	6.02×10^{-4}	4.76×10^{-4}	3.04
37	3.46×10^{-3}	2.14×10^{-3}	1.38×10^{-3}	9.68×10^{-4}	7.00×10^{-4}	5.31×10^{-4}	4.16×10^{-4}	3.18
39	2.94×10^{-3}	1.86×10^{-3}	1.20×10^{-3}	8.47×10^{-4}	6.15×10^{-4}	4.64×10^{-4}	3.62×10^{-4}	3.35
41	2.40×10^{-3}	1.55×10^{-3}	9.97×10^{-4}	7.07×10^{-4}	5.14×10^{-4}	3.87×10^{-4}	3.02×10^{-4}	3.71
43	1.85×10^{-3}	1.22×10^{-3}	7.88×10^{-4}	5.66×10^{-4}	3.05×10^{-4}	3.05×10^{-4}	2.38×10^{-4}	4.01
46	1.45×10^{-3}	9.77×10^{-4}	6.27×10^{-4}	4.47×10^{-4}	3.23×10^{-4}	2.42×10^{-4}	1.88×10^{-4}	4.31
48	1.39×10^{-3}	9.46×10^{-4}	6.00×10^{-4}	4.29×10^{-4}	3.11×10^{-4}	2.32×10^{-4}	1.81×10^{-4}	4.58
51	1.34×10^{-3}	9.30×10^{-4}	5.88×10^{-4}	4.16×10^{-4}	2.98×10^{-4}	2.25×10^{-4}	1.75×10^{-4}	4.83
53	1.19×10^{-3}	8.42×10^{-4}	5.31×10^{-4}	3.77×10^{-4}	2.70×10^{-4}	2.04×10^{-4}	1.58×10^{-4}	4.98
56	7.44×10^{-4}	4.75×10^{-4}	3.33×10^{-4}	2.43×10^{-4}	1.82×10^{-4}	1.43×10^{-4}	1.32×10^{-4}	5.04
57	5.36×10^{-4}	3.49×10^{-4}	2.45×10^{-4}	1.79×10^{-4}	1.35×10^{-4}	1.035×10^{-4}	9.98×10^{-4}	5.31

seen in Table 9. The percentage error of the neutron dose rate for different cells is also given in the last column of Table 9. With the increase in the thickness of the shield, the error rate of the calculations has also increased, but the maximum error rate is below 5%, which is an acceptable error rate in MCNPX calculations. In Table 10, we calculate the gamma dose rates for different thicknesses of shields at different points in the workplace where the IECF is located in order to guarantee the safety of the gamma dose received by the user.

Based on the given data in Table 10, with increasing user distance from the device as well as increasing the thickness of the shield layers, small changes in gamma dose occur. This is due to the fourth layer of lead in the shields which its thickness is fixed at 3 cm based on the calculations of the parameters described in the previous section, such as HVL. In Table 11, we have compared the results of this study, by the name of Faculty of Physics of Isfahan University (FPUI), to the results of shielding for the IECF device at the Brazilian institute of energy and nuclear research (Instituto de Pesquisas Energticas e Nucleares IPEN) at which the simulation of IECF device for the neutron dose was done at three different distances from the device, which is similar to those of our neutron dose measurements. The energy of neutrons in (Lee et al., 2020) is considered 2.5 MeV (due to using D-D as a fuel for fusion), but the energy of neutrons in our study is considered 14.1 MeV (due to using D-T as a fuel as it has a better cross-section of fusion reaction and this fuel was more suitable for our studies in the future). Also, in (Lee et al., 2020) the neutron yield is 10^{12} s^{-1}, while in our work this figure is 10^{9} s^{-1} therefore, there are some differences between the results. The comparison of results is given in Table 10. The reason why we compared the results of our

Table 11: Comparison of our calculations with that of IPEN center.

Distance (cm)	33-67 (D_0)		33-67 (D_{20})		33-67 (D_{40})	
Thickness (cm)	FPUI	IPEN	FPIUI	IPEN	FPUI	IPEN
31	7.65×10^{-2}	3.13×10^{0}	7.65×10^{-2}	2.96×10^{0}	7.65×10^{-2}	2.52×10^{0}
33	5.90×10^{-2}	1.83×10^{0}	5.90×10^{-2}	1.72×10^{0}	5.90×10^{-2}	1.47×10^{0}
35	4.62×10^{-2}	1.07×10^{0}	4.62×10^{-2}	4.62×10^{0}	4.62×10^{-2}	8.42×10^{-1}
37	3.56×10^{-2}	6.31×10^{-1}	3.56×10^{-2}	5.90×10^{-1}	3.56×10^{-2}	4.93×10^{-1}
39	2.72×10^{-2}	–	2.72×10^{-2}	–	2.72×10^{-2}	–
41	2.10×10^{-2}	3.77×10^{-1}	2.10×10^{-2}	3.63×10^{-1}	2.10×10^{-2}	2.92×10^{-1}
43	1.62×10^{-2}	2.21×10^{-1}	1.62×10^{-2}	2.04×10^{-1}	1.62×10^{-2}	1.67×10^{-1}
46	1.10×10^{-2}	1.30×10^{-1}	1.10×10^{-2}	1.18×10^{-1}	1.10×10^{-2}	9.95×10^{-2}
48	8.71×10^{-3}	7.90×10^{-2}	8.71×10^{-3}	7.27×10^{-2}	8.71×10^{-3}	6.10×10^{-2}
51	6.48×10^{-3}	4.58×10^{-2}	6.48×10^{-3}	4.50×10^{-2}	6.48×10^{-3}	3.37×10^{-2}
53	5.31×10^{-3}	2.45×10^{-2}	5.31×10^{-3}	2.04×10^{-2}	5.31×10^{-3}	1.91×10^{-2}
56	2.83×10^{-3}	1.73×10^{-2}	2.83×10^{-3}	1.69×10^{-2}	2.83×10^{-3}	1.24×10^{-2}
57	6.09×10^{-3}	1.01×10^{-2}	6.09×10^{-3}	9.66×10^{-3}	6.09×10^{-3}	7.77×10^{-3}

Table 12: Safe working hours for the IECF device at different times.

Distance (cm)	Dose rate (mSv.year^{-1})	Dosage received by the user in a year (mSv.year^{-1})	Safe working hours in a week (h)	Safe working hours in a year (h)	Dosage received by people in a year (mSv.year^{-1})	Safe hours in a week (h)
28	0.0283072	20	15	706	1	0
54	0.0174999	20	24	1142	1	0
84	0.0120121	20	35	1664	1	1
114	0.0086731	20	48	2305	1	2
154	0.0065226	20	64	3066	1	3

data with the results of (Lee et al., 2020) in three parts is that they used three different ring detectors at three different distances, and we compared our results with the neutron dose results from all three detectors. These rings have a radius of 150 cm and are aligned with the Y-axis as well as the IECF device itself. The coordinates of the centers of these detectors, D_0, D_{20}, D_{40}, are respectively, $(0, 0, 0)$, $(0, 20, 0)$ and $(0, 40, 0)$, given in centimeter. Due to the thickness of 50 cm of air before the shield layers and the thickness of 30 to 63 cm that is suggested for different layers of the shield, at a distance in the range of 33 to 67 cm from the device in the room where the device is located, the neutron dose rate was measured.

The thicknesses of the shield layers that we selected were the closest common thicknesses between the simulations of the two papers. Moreover, in our simulations, in addition to using point and ring detectors, we measured the neutron and gamma dose values by F4 and DF4 tallies for every 30 cm of workspace up to a distance of about 5 meters which is the farthest place from the device. In this comparison, we converted the unit we used from μSv.h^{-1} to rem.h^{-1}. Based on the given data in Table 11, the neutron dose rate decreases as the thickness of the shield layers increases in both simulations. In both simulations, the neutron dose rate also decreases as the user distance from both IECF devices increases. But, the difference between these two simulations is in the amount of reduction of their neutron dose rate at almost common thicknesses. The 39 cm thickness was not compared with (Lee et al., 2020) because there was not the same thickness in it. The best results of the mentioned paper are recorded in D40 detector, which records safer neutron dose rate values. The most important issue for working with the IECF device and using all its many applications is the safe working time with the device at different distances. In Table 12, the safe working hours, according to ICRP60 standards were calculated for IECF device in term of weeks, months and years.

According to the ICRP 60 standard, the maximum safe neutron dose rate for a user working with the device is 20 mSv.year^{-1} for five consecutive years and for people it is 1 mSv.year^{-1}. According to the Fig. 14, we have obtained the total dose rate in steps of 30 cm from the device to a distance of 5 m from it. Based on these results, we have calculated the allowable working hours, according to ICRP 60 for distances from 28 to 154 cm. According to Table 12, the most dangerous distance for the user is 28 cm from the device and less than that. Therefore, if a user is forced for various reasons, she can stay at this distance for about 36 hours but at normal conditions, it is necessary to maintain a distance of one meter from the device for the safety of the device. At distances farther from the device, the user can work more hours with the device. For thicknesses of 154 cm and more, the user is allowed to work with the device for any number of hours.

5 Conclusions

Our calculations show that in this study, the proper shielding for the IECF device when the neutron yield by the device is has done well and IECF device can be used in various applications. The highest dose is related to neutrons, which after passing through the layers of shields, the energy of neutrons and neutron flux decreased well, and af-

ter that, the dose caused by neutrons also decreased completely. This shows that the shield layers have been successful in slowing down the neutrons. Calculations showed that the concrete layer was quite effective in reducing the dose of gamma rays, and the dose caused by gamma after passing through the concrete thickness reduced markedly, and this was one of our goals in choosing the desired concrete as the first layer. In addition, according to the results of Figs. 9 to 11 and the dose rates in the above tables, it can be seen that the neutron dose reduction rate in the first layer of the shield, which contains iron metal, is high. One of the reasons is the presence of iron in this layer, which was very effective because the neutrons produced from the fusion reaction have 14.1 MeV energies and the reduction of this amount of energy to about 3 MeV through inelastic collisions with iron metal is much more than elastic collisions. Therefore our results also well confirm the (DiJulio et al., 2016) results that the presence of metal in the shield, in better and more controlled High-energy neutrons is very effective. Our dosimetry calculations showed that the dose of neutrons and gamma at different distances from the device after the simulated shield is equal to the ICRP60 standard. The environment around the device is safe for employees and ordinary people based on the table provided. Considering the mentioned notes, this device can be used in laboratories, hospitals to produce various radioisotopes for the treatment of various diseases, and in industry as a device for identifying the components of materials and so on. Finally, we compared our simulation results with the shielding simulation of another IECF device (Lee et al., 2020), which improved the results of our study and calculations. In these two papers, the construction of a suitable shield for the IECF device is simulated, and both papers confirm each other's results in terms of neutron and gamma dose reductions, and are also somewhat in agreement with each other in terms of thickness, and have good similarities and despite the difference in the fuel used, their results are in good agreement with each other.

Conflict of Interest

The authors declare no potential conflict of interest regarding the publication of this work.

References

Asadi, A. and Hosseini, S. A. (2021). Investigation of the gamma-ray shielding performance of the B_2O_3-Bi_2O_3-ZnO-Li_2O glasses based on the Monte Carlo approach. *Radiation Physics and Chemistry*, 189:109784.

Bell, G. and Glasstone, S. (1970). Nuclear reactor theory (No. TID-25606). *US Atomic Energy Commission, Washington, DC, US*.

Bevelacqua, J. and Mortazavi, S. (2020). Neutron shielding concrete in medical applications. In *Micro and Nanostructured Composite Materials for Neutron Shielding Applications*, pages 219–237. Elsevier.

Bhattacharjee, D., Buzarbaruah, N., Mohanty, S., et al. (2020). Kinetic characteristics of ions in an inertial electrostatic confinement device. *Physical Review E*, 102(6):063205.

Black, J., Wood-Thanan, M., Maroni, A., et al. (2021). Study of inertial electrostatic confinement fusion using a finite-volume scheme for the one-dimensional Vlasov equation. *Physical Review E*, 103(2):023212.

Buzarbaruah, N., Dutta, N., Bhardwaz, J., et al. (2015). Design of a linear neutron source. *Fusion Engineering and Design*, 90:97–104.

Buzarbaruah, N., Dutta, N., Borgohain, D., et al. (2017). Study on discharge plasma in a cylindrical inertial electrostatic confinement fusion device. *Physics Letters A*, 381(30):2391–2396.

Buzarbaruah, N., Mohanty, S., and Hotta, E. (2018). A study on neutron emission from a cylindrical inertial electrostatic confinement device. *Nuclear Instruments and Methods in Physics Research Section A: Accelerators, Spectrometers, Detectors and Associated Equipment*, 911:66–73.

Chan, Y.-A. and Herdrich, G. (2019). Jet extraction and characterization in an inertial electrostatic confinement device. *Vacuum*, 167:482–489.

Damideh, V., Sadighzadeh, A., Koohi, A., et al. (2012). Experimental study of the Iranian inertial electrostatic confinement fusion device as a continuous neutron generator. *Journal of Fusion energy*, 31:109–111.

De Vries, P. and Gribov, Y. (2019). Iter breakdown and plasma initiation revisited. *Nuclear Fusion*, 59(9):096043.

DiJulio, D., Cooper-Jensen, C. P., Björgvinsdóttir, H., et al. (2016). High-energy in-beam neutron measurements of metal-based shielding for accelerator-driven spallation neutron sources. *Physical Review Accelerators and Beams*, 19(5):053501.

El-Toony, M., Eid, G., Algarni, H., et al. (2020). Synthesis and characterisation of smart poly vinyl ester/Pb_2O_3 nanocomposite for gamma radiation shielding. *Radiation Physics and Chemistry*, 168:108536.

ENDF (2022). Evaluated Nuclear Data File (ENDF). *International Atomic Energy Agency*. https://www-nds.iaea.org.

Farnsworth, P. T. (1966). Electric discharge device for producing interactions between nuclei. US Patent 3,258,402.

Gueibe, C., Rutten, J., Camps, J., et al. (2022). Application of silver-exchanged zeolite for radioxenon mitigation at fission-based medical isotope production facilities. *Process Safety and Environmental Protection*, 158:576–588.

Hu, G., Hu, H., Yang, Q., et al. (2020). Study on the design and experimental verification of multilayer radiation shield against mixed neutrons and γ-rays. *Nuclear Engineering and Technology*, 52(1):178–184.

Hubbell, J. H. and Seltzer, S. M. (1995). Tables of X-ray mass attenuation coefficients and mass energy-absorption coefficients 1 keV to 20 MeV for elements Z= 1 to 92 and 48 additional substances of dosimetric interest. Technical report, National Inst. of Standards and Technology-PL, Gaithersburg, MD.

Kaçal, M., Akman, F., and Sayyed, M. (2019). Evaluation of gamma-ray and neutron attenuation properties of some polymers. *Nuclear Engineering and Technology*, 51(3):818–824.

Lamarsh, J. R. (1966). *Introduction to nuclear reactor theory*. Addison-Wesley.

Lee, S. M., Yoriyaz, H., Cabral, E. L., et al. (2020). Development of neutron shielding for an inertial electrostatic confinement nuclear fusion device.

Mesbahi, A. and Ghiasi, H. (2018). Shielding properties of the ordinary concrete loaded with micro-and nano-particles against neutron and gamma radiations. *Applied Radiation and Isotopes*, 136:27–31.

Miley, G. H. and Murali, S. K. (2014). Inertial electrostatic confinement (IEC) fusion. *Fundamentals and Applications*.

Naseri, A. and Mesbahi, A. (2010). A review on photoneutrons characteristics in radiation therapy with high-energy photon beams. *Reports of Practical Oncology and Radiotherapy*, 15(5):138–144.

Nasrabadi, M. and Baghban, G. (2013). Neutron shielding design for ^{241}Am–Be neutron source considering different sites to achieve maximum thermal and fast neutron flux using MCNPX code. *Annals of Nuclear Energy*, 59:47–52.

Okuno, K. (2005). Neutron shielding material based on colemanite and epoxy resin. *Radiation Protection Dosimetry*, 115(1-4):258–261.

Pelowitz, D. B. et al. (2013). MCNP6 users manual version 1.0. *Los Alamos National Security, USA*.

Pomaro, B., Gramegna, F., Cherubini, R., et al. (2019). Gamma-ray shielding properties of heavyweight concrete with Electric Arc Furnace slag as aggregate: An experimental and numerical study. *Construction and Building Materials*, 200:188–197.

Salehizadeh, A. and Nasrabadi, M. (2021). Modeling of Inertial Electrostatic Confinement device processes for ^{3}He–^{3}He interactions. *Vacuum*, 188:110171.

Santosa, S. and Anggraini, A. (2018). Moderator material efficiency of neutron energy slowing down on D-T reaction neutron generator for SAMOP. In *IOP Conference Series: Materials Science and Engineering*, volume 432, page 012025. IOP Publishing.

Sariyer, D. and Küçer, R. (2018). Development of neutron shielding concrete containing iron content materials. In *AIP Conference Proceedings*, volume 1935, page 100003. AIP Publishing LLC.

Sariyer, D. and Küçer, R. (2020). Effect of different materials to concrete as neutron shielding application. *Acta Phys. Pol. A*, 137(4):477.

Sazali, M. A., Rashid, N. K. A. M., and Hamzah, K. (2019). A review on multilayer radiation shielding. In *IOP Conference Series: Materials Science and Engineering*, volume 555, page 012008. IOP Publishing.

Schmidt, A., Link, A., Welch, D., et al. (2014). Comparisons of dense-plasma-focus kinetic simulations with experimental measurements. *Physical Review E*, 89(6):061101.

Semsari, S., Zakeri, A., Sadighzadeh, A., et al. (2013). Comparison of high-energy He+ and D+ irradiation impact on tungsten surface in the IR-IECF device. *Journal of Fusion Energy*, 32:142–149.

Singh, V. P., Badiger, N., and Vega-Carrillo, H. R. (2015). Neutron kerma coefficients of compounds for shielding and dosimetry. *Annals of Nuclear Energy*, 75:189–192.

Spaeth, M. L., Manes, K. R., Bowers, M., et al. (2016). National ignition facility laser system performance. *Fusion Science and Technology*, 69(1):366–394.

Stone, M. B., Crow, L., Fanelli, V. R., et al. (2019). Characterization of shielding materials used in neutron scattering instrumentation. *Nuclear Instruments and Methods in Physics Research Section A: Accelerators, Spectrometers, Detectors and Associated Equipment*, 946:162708.

Stults, K. A. and Karpius, P. J. (2021). Effects of Shielding on Gamma Rays. Technical report, Los Alamos National Lab.(LANL), Los Alamos, NM (United States).

Syring, C. and Herdrich, G. (2017). Jet extraction modes of inertial electrostatic confinement devices for electric propulsion applications. *Vacuum*, 136:177–183.

Werner, C. (2017). MCNP Users Manual-Code Version 6.2(Report, LA-UR-17-29981). *New Mexico: Los Alamos National Laboratory*.

Werner, C. J., Bull, J., Solomon, C., et al. (2018). MCNP6. 2 release notes. *Los Alamos National Laboratory*.

Zakalek, P., Li, J., Böhm, S., et al. (2021). Tailoring neutron beam properties by target-moderator-reflector optimisation. *Journal of Neutron Research*, 23(2-3):185–200.

Zan, Y., Zhou, Y., Zhao, H., et al. (2020). Enhancing high-temperature strength of (B_4C+ Al_2O_3)/Al designed for neutron absorbing materials by constructing lamellar structure. *Composites Part B: Engineering*, 183:107674.

Zhang, X., Yang, M., Zhang, X., et al. (2017). Enhancing the neutron shielding ability of polyethylene composites with an alternating multi-layered structure. *Composites Science and Technology*, 150:16–23.

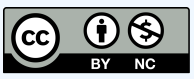

To cite this article:

Zanganeh, H., Nasri Nasrabadi, M. (2023). Simulation of neutron and gamma shielding for an inertial electrostatic confinement fusion device. *Radiation Physics and Engineering*, 4(3), 29-41.
DOI: 10.22034/rpe.2023.384828.1116
To link to this article: https://doi.org/10.22034/rpe.2023.384828.1116